Chemical Engineering Journal 489 (2024) 151281

Contents lists available at ScienceDirect

Chemical Engineering Journal

journal homepage: www.elsevier.com/locate/cej

Internal dry reforming of methane in solid oxide fuel cells

Saeed Moarrefi [a], Mohan Jacob [a], Chao'en Li [b], Weiwei Cai [c], Liyuan Fan [a,*]

[a] College of Science and Engineering, James Cook University, 1 James Cook Drive, Townsville, QLD 4811, Australia
[b] CSIRO Energy, 71 Normanby Road, Clayton North, Victoria 3169, Australia
[c] Hydrogen Energy Technology Innovation Center of Hubei Province, Faculty of Materials Science and Chemistry, China University of Geosciences, Wuhan 430074, Hubei, China

ARTICLE INFO

Keywords:
SOFC
Dry reforming Kinetics
Power-Law
Langmuir–Hinshelwood

ABSTRACT

In the context of global efforts to reduce greenhouse gas emissions and combat extreme global warming, the direct dry reforming of methane reaction in solid oxide fuel cells presents a promising avenue for clean energy production. This study delves into the influence of temperature, gas composition, and current density on the kinetics of dry methane reforming in solid oxide fuel cells. Power Law and Langmuir-Hinshelwood kinetic models were proposed to highlight the impact of operating conditions on dry methane reforming reactions. Results revealed that the feed gas composition strongly affects methane conversion, with higher methane contents resulting in lower conversions. Increasing the CH_4/CO_2 ratio increases reaction rates, and the effect decreases at a ratio of 1.25. The changes in methane concentration on dry methane reforming reaction rate are more significant than those for carbon dioxide. However, increasing carbon dioxide concentration enhances methane conversion. The exothermic nature of CO_2 adsorption suggests that the adsorption process is thermodynamically favourable in dry reforming, and the elevated temperatures generally improve reaction rates and methane conversion by removing carbon deposits and providing the energy needed to break down the chemical bonds in methane which facilitating its transformation. A higher current density significantly enhances the CO_2 adsorption equilibrium constant and further increases methane conversion, highlighting the positive role of electrochemical reactions on dry methane reforming. This study aims to fill the knowledge gap regarding the influence of electrochemical reactions on dry methane reforming behaviours in solid oxide fuel cells, offering critical insights for advancing anode design, thus contributing to the development of solid oxide fuel cell technologies to address global warming and reduce greenhouse gas emissions.

1. Introduction

The 2015 Paris Agreement is a worldwide treaty focusing on reducing greenhouse gases to prevent extreme global warming [1]. On Earth, CH_4 ranks as the second most substantial human-caused greenhouse gas after CO_2, contributing to a 0.6 °C global temperature increase since preindustrial times [2]. Developing technology to convert biogas, a mixture of CH_4 and CO_2 into energy and electricity with minimal emissions is paramount for reducing greenhouse gases [3]. Besides that, syngas is a mixture of CO and H_2 generated through the gasification of carbon-containing materials, can also be utilized as a feedstock for power generation. Next-generation solid oxide fuel cell (SOFC) technology, featuring direct internal reforming (DIR), can efficiently produce energy from biogas and syngas while sequestering carbon from the atmosphere [5]. DIR can be achieved through two primary techniques: steam reforming of methane (SRM) and dry reforming of methane (DRM). SRM, which relies on water vapor, is widely employed but does not directly contribute to CO_2 emission reduction. The need for utility water for steam generation, makes SRM system more complex compared to DRM. Alternatively, the outlet syngas from DRM can be utilized in the fuel cell as the reforming agent. By converting two greenhouse gases (CO_2 and CH_4) into H_2, CO, and electricity, DRM contributes to waste reduction and promotes an overall more direct and simpler industrial process.

Syngas with an H_2/CO molar ratio nearly equal could be generated during the DRM process from biogas, represented by reaction (1) [4].

$$CH_4 + CO_2 \rightleftarrows 2CO + 2H_2 \quad (1)$$

Via reverse water gas shift (RWGS) reaction, H_2 can react with CO_2, leading to the formation of CO and water, represented by reaction (2).

* Corresponding author.
E-mail address: liyuan.fan@jcu.edu.au (L. Fan).

https://doi.org/10.1016/j.cej.2024.151281
Received 24 January 2024; Received in revised form 30 March 2024; Accepted 12 April 2024
Available online 15 April 2024
1385-8947/© 2024 The Authors. Published by Elsevier B.V. This is an open access article under the CC BY license (http://creativecommons.org/licenses/by/4.0/).

Nomenclature

Abbreviations

DRM	Dry Reforming of Methane
SRM	Steam Reforming of Methane
DIR	Direct Internal Reforming
LH	Langmuir-Hinshelwood
RWGS	Reverse Water Gad Shift
SOFC	Solid Oxide Fuel Cell
NiO-YSZ	Nickel-Yttria-Stabilized-Zirconia
NiO-GDC	Nickel-Gadolinium-Doped-Ceria
PL	Power Law
RDS	Rate Determining Step
MFC	Mass Flow Controller
GC	Gas Chromatograph
TPB	Triple Phase Boundary
OCV	Open Circuit Voltage

Latin symbols

P	Constant total pressure, 1 bar
R	Universal gas constant, 8.314 J/(mol K)
T	Temperature, K
k	Reaction Rate constant
a	Reaction order of methane
b	Reaction order of carbon dioxide
R	Methane to Carbon Dioxide Ratio (or CH_4/CO_2)

Subscripts

x_{CH_4}	Overall methane conversion
$F_{CH_4}^{inlet}$	Methane flow rate at the inlet, ml/min
$F_{CH_4}^{outlet}$	Methane flow rate at the outlet, ml/min
W_{cat}	Total weight of the catalyst, g
r_{CH_4}	Reaction rate of methane, mol/s/g
k_0	The pre-exponential factor of rate constant, mol/ (s g bar)
p_j	The partial pressure of species j, bar
K_j	Adsorption equilibrium constant of species j
A_j	The pre-exponential factor of the adsorption constant of species j
ΔH_j	The change of adsorption enthalpy of species j
ΔS_j	The change of entropy of species j
ΔG_j^0	Change of standard Gibbs free energy
K_{eq}	Equilibrium constant of DRM
K_{RWGS}	Equilibrium constant of RWGS
df	Driving force
E_a	Activation energy, kJ/mol

$$CO_2 + H_2 \rightleftarrows CO + H_2O \quad (2)$$

In this system, DRM occurs at the anode's entrance, followed by exothermic electrochemical oxidation of H_2 and CO on the anode, producing electricity following the subsequent reactions (3) and (4) [5,6]:

$$H_2 + O^{-2} \rightarrow H_2O + 2e^- \quad (3)$$

$$CO + O^{-2} \rightarrow CO_2 + 2e^- \quad (4)$$

The anode off-gas can be recycled to the SOFC as an oxidant for the DRM reaction.

DIR-SOFC systems are cost-efficient compared to other fuel cell types by eliminating the need for an external reformer [4,7] exhibiting potential for more thermal resilience, and leveraging electrochemical reactions to induce heat within the functional layer, facilitating efficient fuel reforming. It also shows excellent chemical stability resistance to impurities at atmospheric pressure compared to low temperature fuel cells, accompanied by an adjustable catalytic activity [6,8]. Adjusting catalyst activity in SOFCs is vital for improving efficiency, durability, controlling reactions, and reducing costs, and longer lifespan of this technology. These features position DIR-SOFC as a promising, environmentally friendly energy system capable of mitigating global warming in the future.

However, DIR-SOFCs have drawbacks that reduce their lifespan. The fast internal endothermic reforming process occurs in the SOFCs can cause severe local thermal stress, especially at the entrance, causing long-term performance degradation [9]. Furthermore, the high catalytic activity on the anodes could lead to carbon deposition, which can also cause cell stress and cracks in long-term applications [10]. Further research is needed to improve long-term operation performance [ref].

Current research focuses on enhancing DIR-SOFC system performance through different materials fabrications [6,11–16] and strategies exploring the integration of SOFC within the power generation systems [8,17–20] to assess its techno-economic feasibility [21]. These are crucial steps towards realizing this promising technology into applications. The type of anode materials and the fuel being used impact the fuel cell system performance. Researchers often optimize the anode material to balance electronic conductivity, redox stability, coking and sulfur resistance, temperature resistance, and other factors to maximize the overall efficiency of the SOFC. Table 1 compares the characteristics of the two commonly used anode materials, NiO-GDC (Nickel-Gadolinium Doped Ceria) and NiO-YSZ (Nickel-Yttria Stabilized Zirconia), used in SOFCs. The NiO-YSZ anode shows good electronic conductivity, favorable sintering behavior, and lower cost, while benefiting from easier fabrication method compared to NiO-GDC. Conversely, NiO-GDC offers better redox stability and resistance to coking, making it suitable for using hydrocarbon fuels despite its higher fabrication cost. developing higher electrical conductivity anode materials for SOFCs could lower operating temperatures, enhancing performance and reducing operation cost. Combining the distinct advantages of both materials to develop higher electrical conductivity anode materials could provide a cost-effective approach to balancing operational costs and improving overall SOFC performance.

Controlling the reaction rates and catalytic behaviour of the anode materials are the strategies to avoid carbon deposition and eliminate steep temperature gradients [25]. A thorough study of the kinetics could yield a better understanding of DRM mechanisms and their impact on the performance of the DIR-SOFC system. Most studies related to kinetics consider Power Law (PL) and Langmuir-Hinshelwood (LH) expressions [26]. Fan et al. [27] conducted experiments to explore the impacts of operating temperature, gas composition, current density, and

Table 1
Comparison of NiO-GDC and NiO-YSZ anode materials for SOFCs [5,6,22–24].

Property/ Characteristic	NiO-GDC	NiO-YSZ
Electronic Conductivity	Lower	Higher
Redox Stability	Better	Less favorable
Coking Resistance	More resistant to coking	Prone to coking
Sulfur contamination	Resistant to H2S (~2 ppm)	Prone to sulfur poisoning
Sintering Behavior	Less favorable	Better
Catalytic Activity	Lower	Higher
Cost	More expensive	Relatively less expensive
Ease of Fabrication	Moderate	Easier
Long-Term Stability	Generally Good	Requires Optimization
Applications	Preferred for hydrocarbon fuels	Often used with hydrogen as the fuel

anode thickness on SOFCs utilizing NiO-YSZ electrolyte-supported button cells in SRM process. Both PL and LH kinetic models were used, showing consistent trends in methane and steam partial pressures, a positive reaction order for methane, and a negative influence of steam partial pressure on the reaction rate, with the LH model offering a lower error and higher R^2. Nevertheless, they also observed an inconsistent influence of current density on the H_2O adsorption constant over the NiO-YSZ anode. Zhou et al. [28] extended Fan et al.'s [27] study to explore how variations in current density influence water vapor adsorption behavior on the catalyst surface on a NiO-GDC anode. A notable reduction in the steam adsorption constant was observed in the presence of electrical current. Moreover, among the various current densities investigated, the models exhibited greater accuracy in describing reforming rates at a current density of 600 A/m^2 compared to both open-circuit and 1000 A/m^2 conditions. However, the study was limited to SRM kinetic parameters. Li et al. [18] recently investigated the electrochemical performance and carbon deposition during DRM process in a SOFC. The study indicates that higher CO_2 concentrations can lower the catalyst activity for reforming process and reduce electrochemical performance. Optimal performance, including power density and methane conversion, is achieved at a CH_4/CO_2 ratio of 1. However, the study did not explore the influence of. electrochemical reactions on the DRM reaction kinetic parameters. Thallam Thattai et al. [26] has identified that there is a research gap in understanding the global and intrinsic kinetics of methane reforming for SOFCs. Their study compares PL and LH, highlighting limitations in previous models for NiO-YSZ anodes. Contrary to existing literature, the authors suggests that the methane reforming on metallic (Ni) current collectors may not always be negligible, emphasizing the necessity for further experimental verification. A recent article by Wojcik et al. [29] has further pointed out more complex equations do not always yield more accurate results. Their study concluded that these equations are often applicable within a very narrow temperature range, which should be the main factor when selecting the equation for a specific fuel cell.

Experimental and simulation studies on electrolyte-supported button cells have received significant attention in the literature for their emphasis on understanding overall performance and enhancing catalytic activity [11,26,27]. However, there is limited information available regarding the influence of electrochemical reactions on the kinetics parameters of DRM in SOFCs. Moreover, given the complexity of the reaction mechanisms and the challenges associated with carbon deposition and deactivation of Ni-based anode materials, further research is necessary to identify the factors influencing the DRM, which assists in developing strategies to optimise the fuel cell efficiency. Furthermore, specific kinetic models have been developed to investigate reforming reactions in certain types of SOFCs [30]. However, these models may not precisely describe the reaction orders, adsorption equilibrium constants, and activation energies for all types of materials [27].

This study aims to get the DRM kinetic parameters and the influence of electrochemical reactions on the DRM reaction on a combined NiO-GDC and NiO-YSZ anode, NiO-GDC-YSZ, under various operating conditions. This study seeks to bridge the knowledge gap concerning the impact of electrochemical reactions on DRM catalytic behaviours. Furthermore, these findings provide valuable insights for SOFC anode design under various operational conditions, which could enhance the cell performance, contributing to accelerating the transition to sustainable energy.

2. Experiment

2.1. Electrolyte-supported button SOFC test station

This study's experimental approach closely followed Fan's method [27] in their investigation of SMR models. The experiments were conducted using an electrolyte-supported button cell featuring a combination of NiO-GDC-YSZ anode material (NextCell™). The geometric area of the anode was 0.95 cm^2, with an anode thickness of 50 μm. The function layers of the SOFC button cell are shown in Fig. 1(a). Silver wires (sigmaaldrich) were used for electrical contact, which were attached to the electrodes with silver SOFC ink to ensure proper adherence to the current collectors. The button cell was bonded to an alumina tube using Aremco's high-temperature ceramic adhesives (Ceramabond™ 552). Fuel gas was fed through a smaller alumina tube directly to the anode within the larger tube, as demonstrated in Fig. 1(b).

2.2. Testing procedure

The temperature increase in the tubular furnace to 1073 K at a rate of 2 K/min. The anode is under the nitrogen atmosphere during the heating process [27]. Subsequently, a pure hydrogen stream, saturated with water, was gradually introduced to reduce the environment for the anode at 1073. Gas flow rates were controlled using mass flow controllers (MFC) from Bronkhorst Thermo company, with the total flow rate of 8 nml/min (at $P = 1$ bar and $T = 273$ K). After reducing the cell in pure H_2 for 4 h, hydrogen was replaced with five different biogases compositions as outlined in Table 2. This process was conducted within a temperature range of 1073 K to 1173 K with three current densities. The cathode was exposed to ambient air throughout the experiment.

These biogas compositions vary in the ratio of methane to carbon dioxide (R), allowing for simulations of methane-rich and methane-poor biogas conditions. In the DRM process, carbon deposition can cause anode deactivation [31] during long-term operation. Therefore, the theoretical carbon deposition has been predicted using FactSage. Carbon depositions are anticipated for biogas compositions iii, iv, and v, corresponding to biogas with R value ranging from 1 to 1.5, as shown in Table 2. These predictions are based on equilibrium condition calculations conducted by considering elemental components in the fuel and reaction temperature. The experiment was conducted at three selected temperatures (1073 K, 1123 K, 1173 K), with three different current densities. 0, 500, and 1000 A/m^2 were set under galvanostatic conditions using an Autolab/PGSTAT302N (Metrohm) electrochemical workstation. An extensive moisture removal process involving a condenser and a silica gel desiccant bed was applied to dry the outlet syngas. Subsequently, the dehydrated outlet syngas was analysed by a Shimadzu Nexis Gas Chromatograph (GC-2030) equipped with a TCD detector [27]. The GC was calibrated using gases with known compositions within the same range.

The experiment showed fuel cell voltage variations between 0.9 V and 0.6 V, depending on the current density, representing optimal performance for a kinetic study of biogas-SOFC systems. This aligns with the typical voltage range found in commercial SOFC systems, which ranges from 0.7 V to 1.1 V. Outlet syngas measurements were conducted once the cell temperature and voltage had stabilized, typically after 18 h of continuous operation. This stability ensured consistent gas composition, current density, and cell temperature. The experimental setup is visually represented in Fig. 2.

3. Methodology

The overall methane conversion x_{CH_4} at the anode off-gas outlet is determined by Eq. (1):

$$x_{CH_4} = \frac{F_{CH_4}^{inlet} - F_{CH_4}^{outlet}}{F_{CH_4}^{inlet}} \quad (1)$$

where $F_{CH_4}^{inlet}$ and $F_{CH_4}^{outlet}$ are the CH_4 flowrate at the inlet and outlet, respectively. The methane conversions collected at various temperatures, current densities, and gas compositions will be used to fit in PL and LH kinetics models. These models characterize the electrochemical and catalytic reaction kinetics within SOFCs.

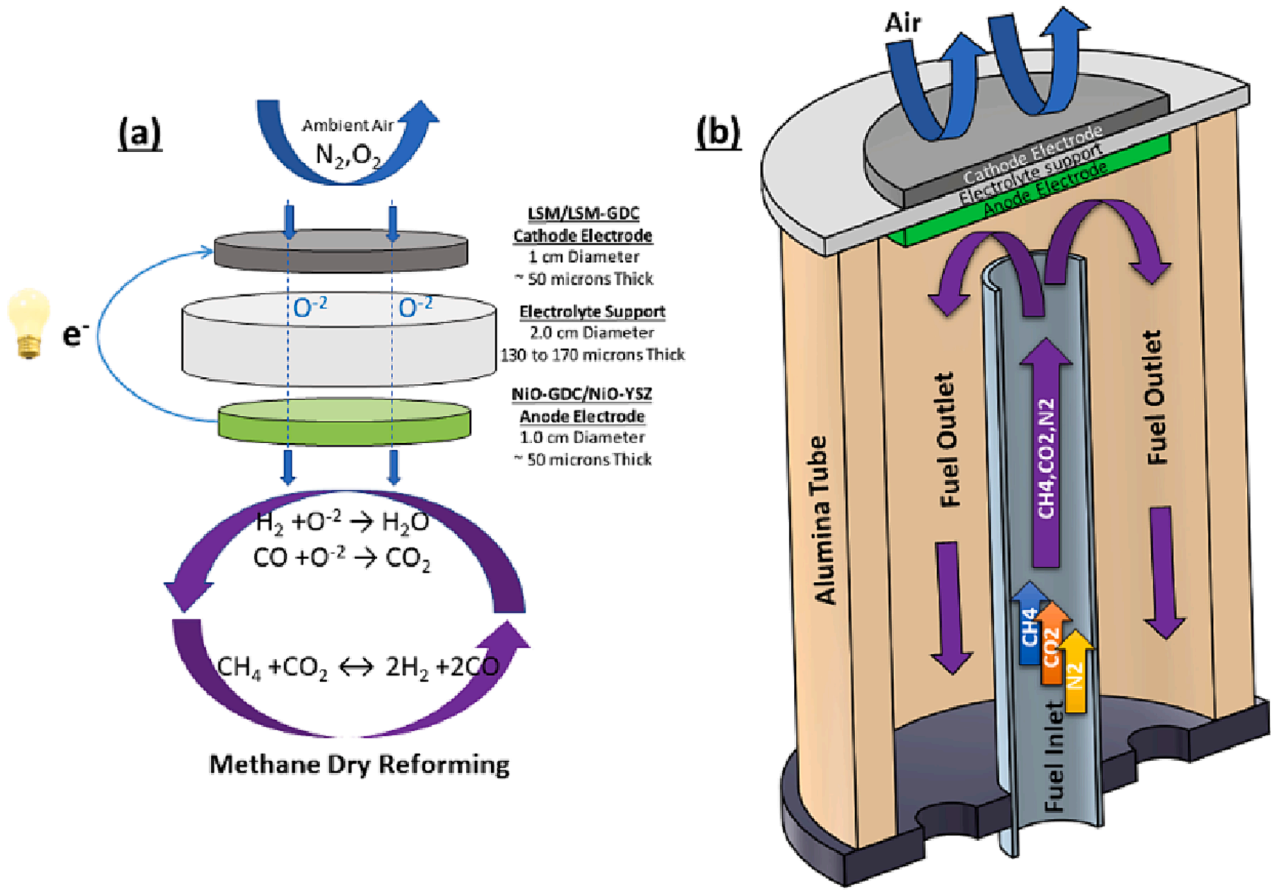

Fig. 1. Schematic illustration of (a) the button fuel cell with NiO-GDC/NiO-YSZ anode; (b) button cell attachment to alumina tube.

Table 2
Inlet biogas compositions and carbon deposition probability at standard conditions.

Case No.	Composition (%)			Total flow rate	CH_4/CO_2	Carbon Deposition (mol C (s))		
	CH_4	CO_2	N_2	nml/min	R	T = 1073 K	T = 1123 K	T = 1173 K
I	30	60	10	8	0.5	0	0	0
Ii	30	40	30	8	0.75	0	0	0
Iii	40	40	20	8	1	0.016	0.005	0
Iv	50	40	10	8	1.25	0.038	0.029	0.025
v	50	33.3	16.7	8	1.5	0.055	0.047	0.044

3.1. Power-law kinetic model

The PL kinetics model is straightforward and convenient to describe homogeneous reactions in which the catalyst and the reactants are present in the same solution or gaseous state. The PL model involves the concentrations of the substances [30], known for being straightforward and practical. However, complex surface chemistry is not considered.

3.2. Langmuir-Hinshelwood kinetics model

Although straightforward and practical, the PL model demonstrates constraints in comprehensively describing diverse reaction mechanisms on heterogeneous catalysts. In contrast, the LH kinetics model is often used to explain reactions occurring on the surface of a catalyst while assuming one of these steps is the Rate-Determining Step (RDS) [26,30]. In this study, surface reactions are observed directly as adsorbed CH_4 and CO_2, rather than as adsorbed elemental and intermediate species of C, H, and O. Therefore adsorption of CH_4 and CO_2 at the surface of catalyst is assumed to be the RDS. The RWGS reaction is much faster than the DRM reaction and is assumed to be at equilibrium [32]. The selected DRM rate equations for both LH and PL models are detailed in Table 3 as follows:

'a' represents the reaction order for methane, while *'b'* denotes the reaction order for carbon dioxide in the rate equation. These coefficients indicate how gas concentrations influence the reaction rate. In the PL model, rate constant k depends on optimizing a and b. In contrast, in the LH model, k relies on optimizing a, b, adsorption coefficient of methane K_{CH_4} and adsorption coefficient of carbon dioxide K_{CO_2}. Table 4 presents the terminology and functions utilized in this study. For a comprehensive understanding of the governing equations and the methodology for mathematical modeling, readers are encouraged to refer to our previous study [27].

3.3. Parameter estimation methodology

The details of the kinetic mechanism, parameter estimation, and model simplification can be found in our previous studies [26–28]. To explore the kinetic of DRM, the Van't Hoff equation was applied to assess the influence of temperature variations on the adsorption coefficient and calculate the corresponding enthalpy and entropy changes, as summarized in Table 4.

Both proposed models were used to estimate reaction orders a and b. The DRM activation energy E_a and pre-exponential factor k_0 were calculated iteratively in MATLAB [33], provided in the Supplementary Material. The reaction orders were constrained between −2 and + 2 to ensure the results remained consistent with values found in the existing

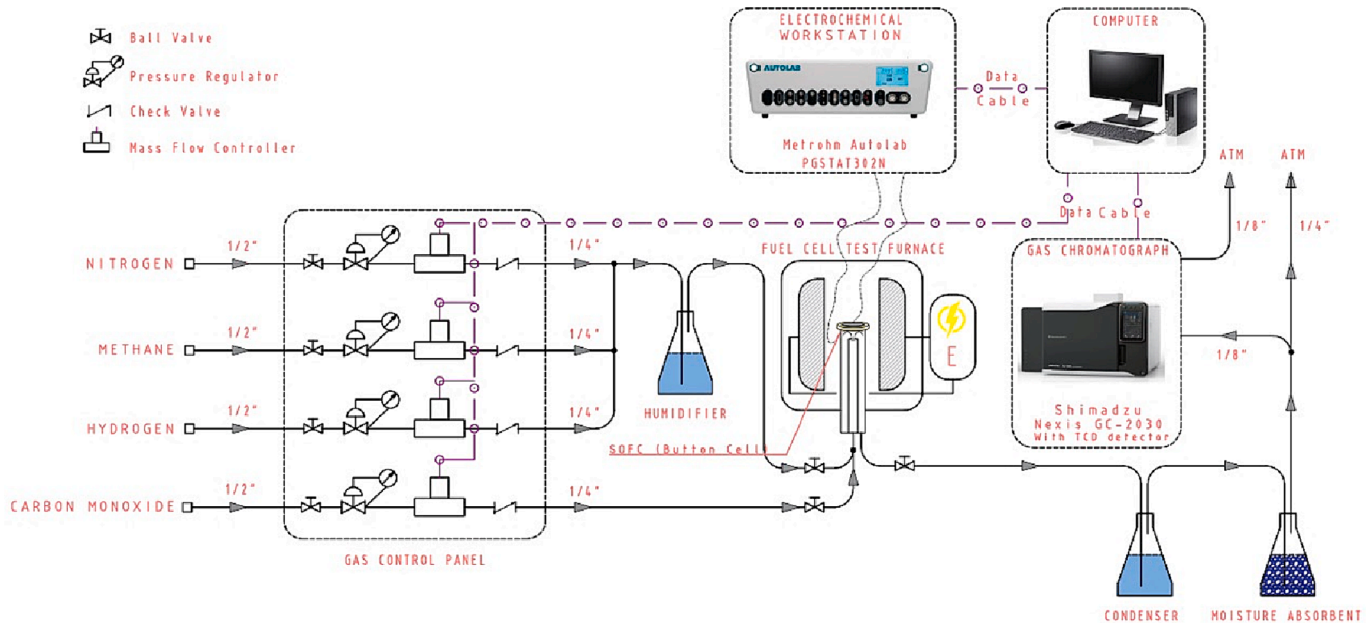

Fig. 2. The experimental test station includes the vertical tube furnace, the fuel cell experiment rig, the gas chromatograph, the electrochemical workstation, the computer, the mass flow controllers, and the pre-treatment and post-treatment facilities for the fuel gas stream.

Table 3
Proposed DRM rate expressions.

Kinetic Model	Reaction Rate Expression	Reaction Rate Constant
PL	$r_{CH_4}^{PL} = k \cdot p_{CH_4}^{a} \cdot p_{CO_2}^{b}$	$k = \frac{F_{CH_4}^{inlet}}{W_{cat}} \int_0^{X_{CH_4}^{outlet}} \frac{1}{r_{CH_4}^{PL}} dX_{CH_4}$
LH	$r_{CH_4}^{LH} = \frac{k p_{CH_4}{}^{a} p_{CO_2}{}^{b}}{\left(1 + K_{CH_4} p_{CH_4} + K_{CO_2} p_{CO_2}\right)^2} \times df$	$k = \frac{F_{CH_4}^{inlet}}{W_{cat}} \int_0^{X_{CH_4}^{outlet}} \frac{1}{r_{CH_4}^{LH}} dX_{CH_4}$

Table 4
Terms and functions considered in this study.

Term	Function	Definition
K_{DRM}^{eq}	$6.78 \cdot 10^{14} \cdot \exp(\frac{-259660}{RT})$	The equilibrium constant of DRM
K_{RWGS}^{eq}	$56.971 \cdot \exp(\frac{-35580}{RT})$	The equilibrium constant of RWGS
df	$1 - \frac{p_{CO}{}^2 p_{H_2}^2}{K_{DRM}^{eq} p_{CH_4} p_{CO_2}}$	Driving force
A_{CH_4}	0.000665	The pre-exponential factor of methane adsorption
$\Delta H_{CH_4}^0$	−38.28	Change of adsorption enthalpy (kJ/mol)
R	8.314	Universal gas constant (J/ (mol K))
W_{cat}	14.3	Catalyst total weight (mg)
K_j	$\exp(-\frac{\Delta G_j}{RT}) = A_j \cdot \exp(-\frac{\Delta H_j}{RT})$	Van't Hoff equation for adsorption coefficient
k	$k_0 \exp(\frac{-E_a^{DRM}}{RT})$	Arrhenius equation for rate constant for DRM
ΔG_j^0	$\Delta G_j^0 = \Delta H_j^0 - T\Delta S_j^0$	Change of Gibbs free energy
ΔS_{ad}^0	$\log(A_d) \times R$	Change of entropy for adsorption

literature [4]. After determining the reaction rate constants at various temperatures, the activation energy can be computed by fitting the following linear equation derived from Arrhenius Eq. (2).

$$\ln(k) = \ln(k_0) - \frac{E_a}{R} \cdot \frac{1}{T} \tag{2}$$

Rules and guidelines are used to evaluate the validity of the Langmuirian kinetics. The adsorption equilibrium constants were assessed based on thermodynamic parameters. This process helps evaluate rate expressions. The rules include the requirement for exothermic adsorption ($-\Delta H_j^0 > 0$), decrease in entropy after adsorption ($-\Delta S_j^0 > 0$), and the constraint that an adsorbing species can't lose more entropy than it initially possesses ($\Delta S_j^0 < -42 \mathrm{J/(mol\,K)}$ and $A_j \leq 0.0064$) [26,27,34].

4. Results and discussion

This study aims to understand the electrocatalytic behaviour of a button SOFC via the DRM process, using NiO-GDC-YSZ as the anode material under various operating conditions. The first section of this study examines the influence of fundamental operational parameters, such as temperature, gas composition, and current density, on the overall methane conversion and reaction rate. The following sections explore how current density and other factors affect the kinetic parameters for both the LH and PL kinetic models. Some kinetic parameters reported previously are not comparable due to the varied anode materials and process conditions. In the following sections, we will focus on the trend of how operating conditions influence the DRM kinetics.

4.1. Effect of operational conditions on dry methane reforming

Methane conversions under different operational conditions can be found in Table 5 and the influence of the fuel composition, current density and operating temperature on the methane conversion is shown in Fig. 3. These graphs have been generated through calculations based on the methane conversion equation provided in Eq. (1).

DRM reaction rate refers to the speed at which the concentration of methane, carbon dioxide, or other products change per unit of time per catalyst weight [28]. These rates are influenced by the reactant concentration, temperature, surface area, catalysts, and the reaction mechanism. However, when considering electrochemical reactions with the application of current density in SOFCs, electrochemical reactions promote charge transfer across an interface, and the reaction rates can

Table 5
Methane conversions under various operational conditions.

Temperature [K]	Current Density [A/m^2]	Overall Methane Conversion (%)				
		i	ii	iii	iv	v
1073	0	21.90	20.60	18.40	17.30	17.20
	500	23.40	22.20	19.50	18.70	18.10
	1000	25.80	24.60	21.90	20.30	19.90
1123	0	24.10	22.80	20.10	19.00	18.90
	500	25.20	24.00	22.20	20.40	19.90
	1000	27.40	26.20	23.90	22.00	21.60
1173						
	0	22.10	21.90	21.80	21.60	21.40
	500	23.00	22.80	21.90	21.70	21.60
	1000	26.20	25.10	24.00	22.80	22.50

be also influenced. In Table 6, the gas composition case labelled as v with R of 1.5 and a higher current density demonstrates a notably higher reaction rate than other cases and operating conditions in this experiment.

4.1.1. CH_4/CO_2 feeding ratio

The decrease in methane conversion as the methane partial pressure increases is depicted in Fig. 3. It was also found that this effect is consistent across all current densities and temperatures in the DRM on SOFC. The reaction rate value observed in this study closely matches that of a previous study conducted by Moon et al. [35]. The trend is also similar to Fan et al.'s study [27] but the magnitude of reaction rate is not comparable due to the varied anode materials and experimental conditions. This effect may be attributed to the mass action law, where higher methane concentrations can lead to unwanted side reactions or catalyst saturation, reducing overall conversion efficiency [36]. Conversely, lowering the molar fraction of methane in the gas mixture enhances conversion by promoting a more favourable distribution of reactants on the catalyst's surface, reducing unwanted side reactions, and improving selectivity [37]. Increasing the partial pressure of carbon dioxide as an active oxidant positively influences methane conversion, as evidenced by prior research [35,38]. This trend suggests that excess carbon dioxide can facilitate methane conversion to hydrogen and carbon monoxide, restoring a new equilibrium state to counteract the excess carbon dioxide [39,40]. The trend of methane conversion obtained in this study closely matches that of previous investigations conducted by Chein et al. [41].

The experiment result showed that increasing the CH_4/CO_2 feeding ratio increases the reaction rate due to competitive adsorption of CH_4 and CO_2 on the catalyst surface. It was observed that there is a positive impact of methane partial pressure on the DRM reaction, and this enhancement levels off for values above R = 1.25. Beyond this point, further increases in methane partial pressure do not positively impact reaction rates. This could imply the adsorption competition between the methane and carbon dioxide molecules on the catalytic sites. However, the trend was flatter when the R ratio was low and significantly rising when the R ratio further increased, then levelled off for values above R = 1.25, as shown in Fig. 4. The CH_4/CO_2 feeding ratio in SOFCs is critical for optimizing fuel utilization electrochemical reactions and preventing issues like carbon deposition. An imbalanced ratio can result in incomplete fuel conversion and reduced electrochemical efficiency, leading to carbon deposition, which can foul the anode and reduce its performance [42]. The fuel ratio can affect the redox state of the anode material, impacting its ability to conduct charge and participate in electrochemical reactions [43]. Finding the right balance in this ratio helps prevent carbon buildup and maintains long-term cell performance and efficiency in solid oxide fuel cells [5].

Some researchers have proposed that maintaining a CH_4 to CO_2 ratio 1:1 is essential for achieving maximum methane conversion and promoting efficient syngas production [44]. This optimal ratio is pivotal in influencing the reaction rate during DRM. Any deviations from this ideal ratio can lead to decreased reaction rates, emphasizing the complex interplay of these factors in governing the DRM reaction rate.

4.1.2. Current density

Fig. 3 also displays the current density-dependent methane conversions in this study, suggesting that electric current significantly enhances methane conversion, demonstrating the positive effect of electrochemical reactions on the DRM reaction. Similar to the study of Saadabadi et al. [44], our results also indicate an increase in current

Table 6
Specific reaction rates for DRM under different operating conditions: temperature ranging from 1073 K to 1173 K and current density varying from 0 to 1000 A/m^2.

Temperature [K]	Current Density [A/m^2]	$r_{CH_4} \times 10^{-3}$ mol/s.g				
		i	ii	iii	iv	v
1073	0	1.64	1.54	1.84	2.16	2.15
	500	1.75	1.66	1.95	2.34	2.26
	1000	1.93	1.84	2.19	2.53	2.49
1123	0	1.81	1.71	2.01	2.37	2.36
	500	1.89	1.80	2.22	2.55	2.49
	1000	2.05	1.96	2.39	2.75	2.70
1173						
	0	1.66	1.64	2.18	2.70	2.67
	500	1.72	1.71	2.19	2.71	2.70
	1000	1.96	1.88	2.40	2.85	2.81

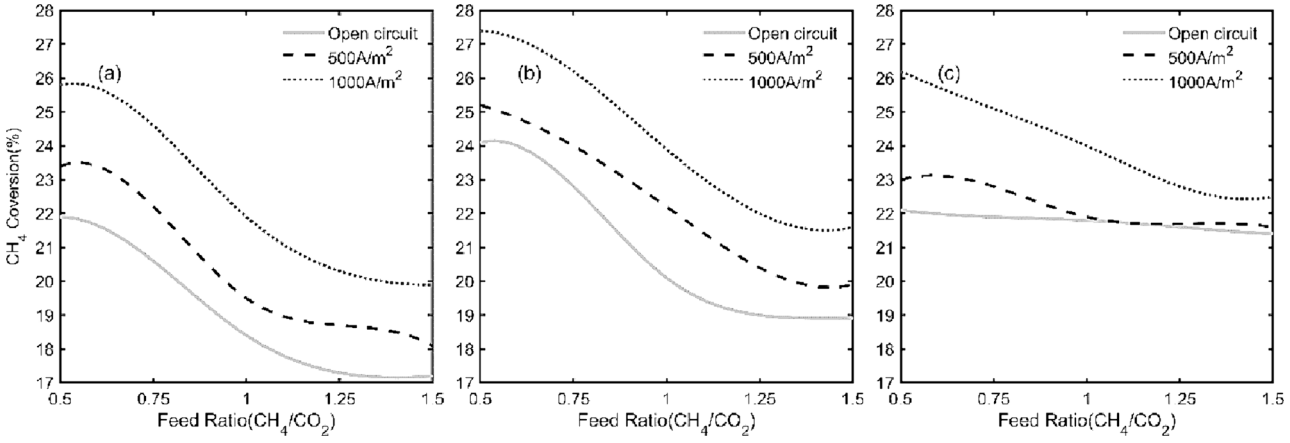

Fig. 3. Feed ratio-dependent methane conversion behavior at (a)1073 K, (b)1123 K, (c)1173 K, (d). The solid line corresponds to 1000 A/m^2, the dashed line related to 500 A/m^2, and the dotted lines correspond to OCV.

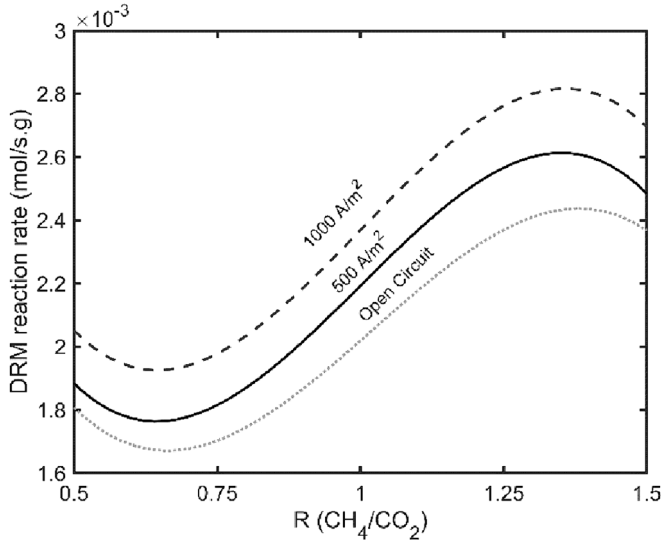

Fig. 4. The DRM reaction rate at 1123 K with various current densities and R ratios. The dashed line corresponds to 1000 A/m^2, the solid line related to 500 A/m^2, and the dotted lines correspond to OCV.

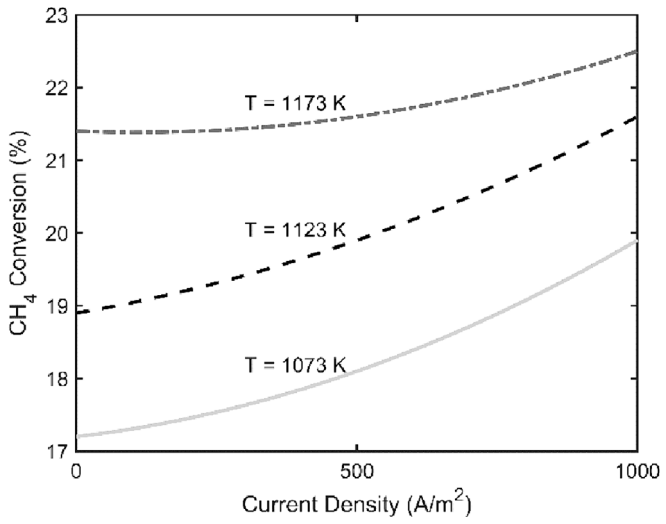

Fig. 5. Temperature-dependent methane conversion behavior for gas composition v at R = 1.5 with current density ranging from 0 to 1000 A/m^2. The solid line corresponds to 1073 K, the dashed line related to 1123 K, and the dash-dotted lines correspond to 1173 K.

density signifies a higher flow of electrons from the anode to the cathode in the SOFC. Lyu et al. found in their work [24] that the current density can be readily translated into the oxygen flow rate, actively involved in the thermodynamic equilibrium of the anode fuel gas, demonstrating that elevated electron flow intensifies the electrochemical activity at the catalyst surface. Methane molecules undergo oxidation, breaking down into CO_2 and H_2O in the presence of oxygen ions derived from the electrolyte [45]. Also, other researchers found that the oxidation reaction becomes more robust as more electrons are drawn out of the anode due to the heightened current density [5,28,46]. An alternate hypothesis suggests that increasing current density within an SOFC can create temperature gradients across the catalyst's surface [47]. This effect is primarily due to the higher electron flow resulting from increased current density. As more electrons are drawn through the SOFC, some regions of the catalyst may become hotter than others, causing temperature variations [30]. Specifically, localized areas with higher temperatures can facilitate endothermic catalytic reactions, ultimately enhancing the conversion of methane into products. However, drawing higher current density from the cell induces thermal stress, potentially causing mechanical strain that could impact the cell's structural integrity over time [25].

The DRM reaction rate also exhibits an increase when a current is applied. An example at 1123 K has been shown in Fig. 4. Our finding supports the idea that a higher current, leading to increased oxygen ion flux at the triple phase boundary (TPB), helps boost the DRM reaction rate [28,50,51]. Consequently, consumption of hydrogen ions could shift the DRM reaction equilibrium towards higher conversion, and the competitive adsorption between methane and carbon dioxide molecules impedes a further increase in the DRM reaction rate through the electrochemical reaction [23,52,53]. Furthermore, increasing current density creates a higher temperature gradient through TPB, which may facilitate the charge carrier transport and overall SRM reaction kinetics [54] as observed by Zhou et al. [28], may also apply to DRM reactions.

4.1.3. Temperature

The experiment results reveal that a higher temperature yields a higher conversion. The temperature and current dependence of methane conversion at a constant R-value of 1.5 is depicted in Fig. 5. Operating temperature strongly affects methane conversion, with higher temperatures leading to increased conversion due to the thermodynamically favoured removal of carbon deposits from the catalyst surface [48,49], driving the conversion of methane into carbon dioxide and water [50]. Similar to the influence of current density described in the previous section, this elevated temperature could provide the necessary energy to promote the DRM reaction [51]. Previous studies have shown a consistent positive correlation between temperature and methane conversion, while temperatures above 1023 K are particularly advantageous for minimizing coke deposition during the DRM process [52].

In line with prior research by Fan et al. [27] on SRM, our finding shows that elevated temperatures can positively affect DRM reaction rates. The potential reasons for the increase in reaction rate with temperature enhancement, as outlined in Table 6, could be attributed to several factors: (1) higher temperatures increase particle kinetic energy, promoting faster reactant diffusion, more collisions, and a higher reaction rate; (2) elevated temperatures enhance ionic and electronic conductivity in SOFC materials, facilitating charge carrier transport and overall reaction kinetics; (3) Increasing temperature lowers the activation energy barrier for reactions, particularly relevant for electrode and oxygen ion transport reactions in SOFCs [52]; (4) Higher temperatures might enhance the accessibility of reactant molecules to active sites on the catalyst surface, promoting more interactions and increasing reaction rates. Lower temperatures can lead to slower reaction rates and reduced cell performance [10].

4.2. Effects of electrochemical reaction on dry methane reforming kinetics

In this study, data fitting has been used to analysis the kinetic parameters [33]. The optimization process for determining reaction rate constants and absorption kinetics can be found in the previous literature [26–28,34,53]. To predict reaction rate constants and absorption kinetics, we utilized the "fmincon" function in MATLAB, employing the "interior-point" algorithm to find the best-fit values for these parameters. This approach considers various experimental data and constraints, as outlined in section 4. The derived DRM kinetic parameters including the reaction orders, activation energy, and the pre-exponential factor for PL and LH models are listed in Table 7.

Positive reaction orders predicted by both models are observed at various current densities. The reaction order of CH_4 agrees with another kinetic studies [27,28,34] which are between 0.5 and 1 while showing same dependencies on the current density. The lack of data regarding the reaction order of CO_2 in DRM reactions on SOFCs makes direct comparisons impossible, but it serves as a good starting point to this

Table 7
Derived kinetic parameters for PL and LH models and variation in CO2 adsorption parameters across different current densities.

Kinetic Parameters	Current Density [A/m^2]	PL	LH
a	**Open-Circuit**	0.85	1
	500	0.98	1
	1000	0.99	1
b	**Open-Circuit**	0.58	0.61
	500	0.59	0.58
	1000	0.54	0.54
E_a (kJ/mol)	**Open-Circuit**	21.82	21.4
	500	15.57	14.4
	1000	13.35	12.1
K_0 (mol/s g bar$^{(a+b)}$)	**Open-Circuit**	0.10	0.12
	500	0.06	0.06
	1000	0.06	0.05
K_{CO_2}	**Open-Circuit**	–	1.25E-07
	500	–	1.65E-07
	1000	–	4.35E-07
A_{CO_2}	**Open-Circuit**	–	4.18E-08
	500	–	5.15E-08
	1000	–	1.45E-07
$\Delta H^0_{CO_2}$ (kJ/mol)	**Open-Circuit**	–	−10.7
	500	–	−11.4
	1000	–	−10.7
$\Delta S^0_{CO_2}$ (kJ/mol. K)	**Open-Circuit**	–	−141.2
	500	–	−139.5
	1000	–	−130.9

research field. The magnitude of these reaction orders indicates that the reaction rate of DRM is more affected by changes in the concentration of methane than by carbon dioxide. Increasing the current density enhances the significance of methane in the electrochemical reaction rate, as seen in Fig. 6, while carbon dioxide's impact decreases slightly. This phenomenon can be explained by the influence of current density on reaction kinetics [25], when higher current densities are drawn from the fuel cell, electrochemical activity at the anode increases. This heightened electron flow enhances methane oxidation, resulting in a more efficient conversion of methane into carbon dioxide and water [54]. In the LH model, the predicted reaction orders were higher, especially when under open-circuit conditions.

Fig. 6 also demonstrates the influence of electrochemical reaction on the activation energy, showing a decrease of nearly 1.7 times from OCV to 1000 A/m^2. This reduction highlights a significant decline in the energy barrier for methane and carbon dioxide molecules to transition into products, even with a low current density. Our findings align with prior studies by Thattai et al. [26] and van Biert et al. [34] in the SRM process, demonstrating analogous trends. Furthermore, the same trend was observed by Fan et al. [27] and Zhou et al. [28] in their studies. This consistency in SRM suggests the possibility of a similar occurrence in the DRM process as well. The potential reasons are: (1) applying an external current or potential difference across an electrochemical cell in an electrochemical reaction can drive non-spontaneous chemical reactions. This current effectively lowers the activation energy barrier by providing the necessary energy for the reaction to proceed [13]. (2) Electrochemical reactions can also influence the activation energy by acting as catalysts. Electrocatalysts can facilitate electrochemical reactions by providing an alternative reaction pathway with a lower activation energy [55]. Considering this definition, SOFC is an electrocatalyst material that provides faster reactions and makes them more favorable. (3) Higher local temperatures resulted from electrochemical reactions can promote the DRM reactions [22].

In the LH model, the calculated activation energy value was lower than the PL model with the same current density. Numerous researchers used LH models when extracting kinetic parameters in catalytic reactions [28,43,56–58]. This is because the LH model considers surface reaction mechanism. In catalytic DRM, the main steps include the adsorption of CH_4 and CO_2, their surface reactions to produce H_2 and CO and the desorption of the syngas products [13,58]. In the adsorption step, the adsorption equilibrium constant (K_j) represents the affinity of reactant molecules to bind to the catalyst surface [51]. A higher K_{CO_2} indicates stronger CO_2 adsorption in that specific current density level, influencing the reaction rate and selectivity, making it a valuable factor for designing and improving catalytic processes [30]. The change in enthalpy and entropy of CO_2 adsorption in a DRM reaction provides essential insights into the thermodynamics of the adsorption process [25,32,52,54]. The calculated adsorption equilibrium constant, its pre-

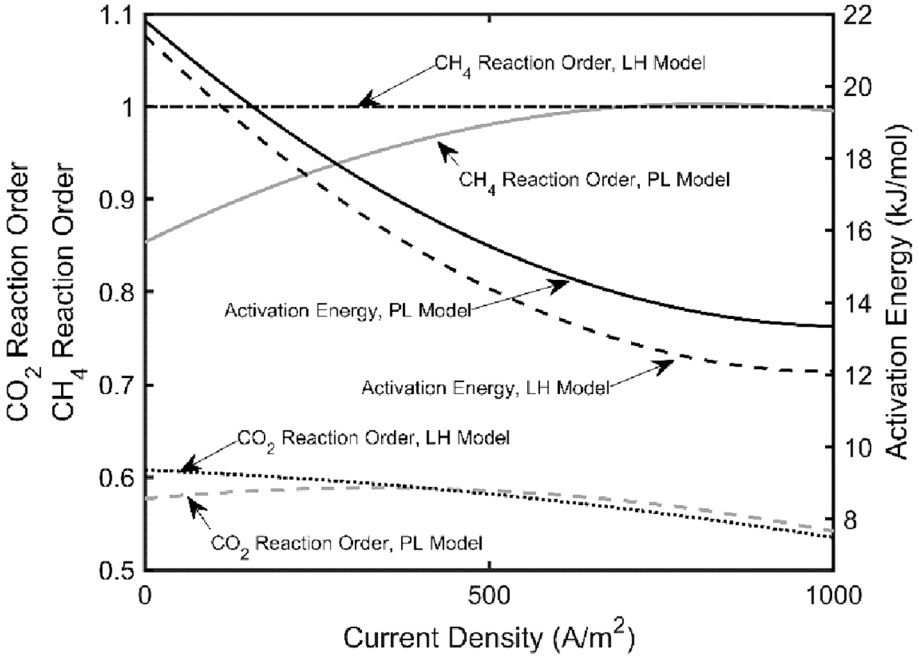

Fig. 6. Trend analysis of current density effects on reaction orders for CH_4 and CO_2, along with activation energy. The dash-dotted line corresponds to a in LH model, the black solid line related to E_a in PL model, the black dash line corresponds to E_a in LH model, the gray solid line represent a in PL model, the dotted line correspond to b in LH model and gray dashed line related to b in PL model.

exponential factor, and the quantity of the enthalpy and entropy of CO_2 adsorption are also available in Table 7. The trends are shown in Fig. 7. Increasing the current density from OCV to 1000 A/m^2 resulted in a four-time increase in the CO_2 adsorption equilibrium constant, underscoring the notable impact of current density on the adsorption constant. A negative $\Delta H^0_{CO_2}$ indicates an exothermic adsorption process, where heat is released as CO_2 molecules adsorb onto the catalyst surface. This indicates that the adsorption of CO_2 is thermodynamically favourable. Additionally, the observed trends suggest that elevating the current density slightly impacts the changes in enthalpy values for CO_2 species. A negative $\Delta S^0_{CO_2}$ indicates a decrease in disorder or a more ordered state during CO_2 adsorption. The increase in entropy by 10 kJ/(mol · K) resulting from the current draw in the fuel cell suggests a stronger attachment of CO_2 molecules to specific sites on the catalyst surface. This leads to a more organized state compared to the open circuit condition.

5. Conclusions

We investigated DRM within an electrolyte-supported NiO-GDC-YSZ button SOFC, focusing on the effects of various operating conditions on the reaction rate and the influence of the electrochemical reaction on the kinetics. A higher CH_4 partial pressure results in a reduced conversion, whereas an increased partial pressure of CO_2 has a positive impact on the overall methane conversion. Operating temperature significantly affects the overall methane conversion, higher temperatures increased the methane conversions possibly due to the efficient removal of carbon deposits from the catalyst surface and energy provision to the endothermic DRM reactions, as well as the change of various reaction equilibriums. Increasing temperature also positively impacts reaction rates, attributed to improved reactant diffusion effect and overall reaction rate constant. Proper feedingCH_4/CO_2 ratio in SOFCs is important for optimizing fuel utilization and prevent issues such as carbon deposition. An imbalanced ratio can lead to incomplete fuel conversion and decreased electrochemical efficiency, affecting overall cell performance. Our findings reveal that increasing the CH_4/CO_2 ratio positively impacts the reaction rate, although this effect levels off beyond a certain point.

Moreover, we have presented kinetic parameters for DRM using both the PL and LH models. These parameters, encompassing reaction orders, activation energy, and pre-exponential factors, have shed light on the influence of electrochemical reactions. Applying a current density in SOFCs, with the flux of oxygen ions at the TPB, promotes the DRM reaction. Also, we found that a higher current density further enhanced the methane conversion, demonstrating that the electron flow and oxygen ion flux could benefit the conversion of CH_4. Current density has a substantial effect on the role of methane in the reaction rate, emphasizing its importance in DRM kinetics. Furthermore, we have explored DRM adsorption parameters which a higher K_{CO_2} signifies stronger adsorption, impacting the reaction rate and selectivity. Additionally, we have discussed the enthalpy and entropy changes during CO_2 adsorption, offering valuable insights into the thermodynamics of DRM.

Since the reforming agent for DRM differs from SRM, comparing data between these two processes poses challenges. However, we observed similarities between SRM and DRM kinetic parameters under certain conditions, prompting further investigation to identify underlying reasons. Comparing results of this study with others revealed increased methane conversion with increasing current density and temperature in both processes, along with increased reaction rates. Despite differences in temperature range, process condition and fuel cells used, both SRM and DRM exhibit a reduction in activation energy for methane reforming, even at a low current density. While the magnitude of the methane reaction order differs between the two processes, both exhibit an increase in methane reaction order with an elevation when a current is drawn. Increasing the partial pressure of CO_2 enhances methane conversion in DRM, which has been also observed in other studies. These findings contribute to our understanding of DRM in SOFC, providing essential parameters for designing an improved electrocatalytic processes. However, a significant research gap exists in comprehensively examining the impact of electrochemical reactions on catalytic behavior in both DRM and SRM processes, highlighting the need for further research.

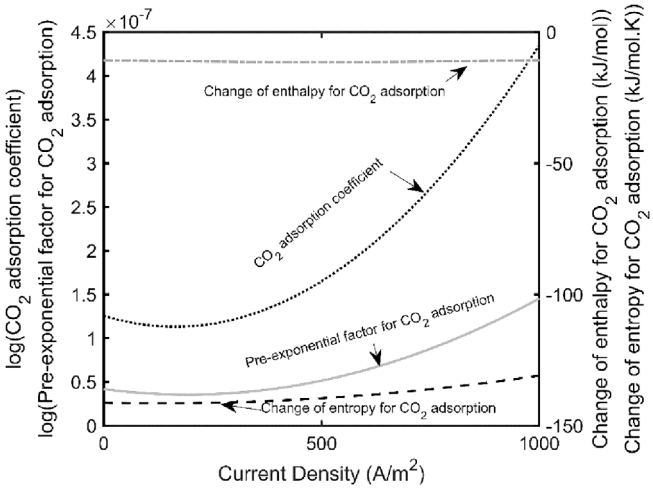

Fig. 7. Trend analysis of current density influences on CO_2 adsorption parameters. The dash-dotted line corresponds to $\Delta H^0_{CO_2}$, the dotted line related to $\mathrm{Log}(K_{CO_2})$, the gray solid line represents $\mathrm{Log}(A_{CO_2})$ and the dashed line correspond to $\Delta S^0_{CO_2}$.

CRediT authorship contribution statement

Saeed Moarrefi: Writing – original draft, Software, Investigation, Formal analysis, Data curation. **Mohan Jacob:** Supervision, Resources. **Chao'en Li:** Writing – review & editing, Supervision, Methodology, Formal analysis. **Weiwei Cai:** Writing – review & editing, Supervision, Investigation. **Liyuan Fan:** Writing – review & editing, Supervision, Resources, Project administration, Methodology, Investigation, Formal analysis, Conceptualization.

Declaration of competing interest

The authors declare that they have no known competing financial interests or personal relationships that could have appeared to influence the work reported in this paper.

Data availability

Data will be made available on request.

Acknowledgement

The authors would like to thank James Cook University, Australia, for providing the education and resources support. This research received no specific grant from funding agencies in the public, commercial, or not-for-profit sectors.

Appendix A. Supplementary data

Supplementary data to this article can be found online at https://doi.org/10.1016/j.cej.2024.151281.

References

[1] M. Meinshausen, J. Lewis, C. McGlade, J. Gütschow, Z. Nicholls, R. Burdon, L. Cozzi, B. Hackmann, Realization of paris agreement pledges may limit warming

just below 2 °C, Nature 604 (7905) (2022) 304–309, https://doi.org/10.1038/s41586-022-04553-z.
[2] L. Shen, D.J. Jacob, R. Gautam, M. Omara, T.R. Scarpelli, A. Lorente, D. Zavala-Araiza, X. Lu, Z. Chen, J. Lin, National quantifications of methane emissions from fuel exploitation using high resolution inversions of satellite observations, Nat. Commun. 14 (1) (2023) 4948, https://doi.org/10.1038/s41467-023-40671-6.
[3] D.S.S.S. Sirigina, A. Goel, S.M. Nazir, Process concepts and analysis for co-removing methane and carbon dioxide from the atmosphere, Sci. Rep. 13 (1) (2023) 17290, https://doi.org/10.1038/s41598-023-44582-w.
[4] L. Fan, C.E. Li, L. van Biert, S.-H. Zhou, A.N. Tabish, A. Mokhov, P.V. Aravind, W. Cai, Advances on methane reforming in solid oxide fuel cells, Renew. Sustain. Energy Rev. 166 (2022) 112646, https://doi.org/10.1016/j.rser.2022.112646.
[5] L. Fan, C.E. Li, P.V. Aravind, W. Cai, M. Han, N. Brandon, Methane reforming in solid oxide fuel cells: challenges and strategies, J. Power Sources 538 (2022), https://doi.org/10.1016/j.jpowsour.2022.231573.
[6] I. Aznam, A. Muchtar, M.R. Somalu, N.A. Baharuddin, N.A.H. Rosli, Advanced materials for heterogeneous catalysis: a comprehensive review of spinel materials for direct internal reforming of methane in solid oxide fuel cell, Chem. Eng. J. 471 (2023) 144751, https://doi.org/10.1016/j.cej.2023.144751.
[7] E. le Saché, T.R. Reina, Analysis of dry reforming as direct route for gas phase CO2 conversion. the past, the present and future of catalytic DRM technologies, Progress Energy Combustion Sci. 89 (2022) 100970, https://doi.org/10.1016/j.pecs.2021.100970.
[8] E.V. Tsipis, D.A. Agarkov, Y.A. Borisov, S.V. Kiseleva, A.B. Tarasenko, S. I. Bredikhin, V.V. Kharton, Waste gas utilization potential for solid oxide fuel cells: a brief review, Renew. Sustain. Energy Rev. 188 (2023) 113880, https://doi.org/10.1016/j.rser.2023.113880.
[9] M.S. Khan, Y. Miura, Y. Fukuyama, S. Gao, Z. Zhu, Methane internal steam reforming in solid oxide fuel cells at intermediate temperatures, Int. J. Hydrogen Energy 47 (29) (2022) 13969–13979, https://doi.org/10.1016/j.ijhydene.2022.02.128.
[10] Y. Bae, J. Hong, Enhancement of surface morphology and catalytic kinetics of NiAl2O4 spinel-derived Ni catalyst to promote dry reforming of methane at low temperature for the direct application to a solid oxide fuel cell, Chem. Eng. J. 446 (2022) 136978, https://doi.org/10.1016/j.cej.2022.136978.
[11] P. Qiu, L. Wu, K. Cheng, S. Wu, H. Qi, C. Xiong, B. Tu, Ni-doped Ba0.9Zr0.8Y0.2O3-δ as a methane dry reforming catalyst for direct CH4–CO2 solid oxide fuel cells, Int. J. Hydrogen Energy 48 (71) (2023) 27805–27813, https://doi.org/10.1016/j.ijhydene.2023.03.391.
[12] A. Nishimura, Y. Hayashi, S. Ito, M.L. Kolhe, Performance analysis of hydrogen production for a solid oxide fuel cell system using a biogas dry reforming membrane reactor with Ni and Ni/Cr catalysts, Fuels 4 (3) (2023) 295–313.
[13] L. Pino, C. Italiano, M. Laganà, A. Vita, V. Recupero, Kinetic study of the methane dry (CO2) reforming reaction over the Ce0.70La0.20Ni0.10O2−δ catalyst, Catal. Sci. Technol. 10 (8) (2020) 2652–2662, https://doi.org/10.1039/C9CY02192B.
[14] J. Zhang, M. Li, F. Jin, J. Zhang, R. Li, X. Li, Y. Gao, X. Ou, Y. Ling, Direct carbon dioxide-methane solid oxide fuel cells combined with in-situ exsolution perovskite La0.75Sr0.25Cr0.5Fe0.4Cu0.1O3-δ-based dry reforming catalysts, Int. J. Hydrogen Energy 55 (2024) 572–580, https://doi.org/10.1016/j.ijhydene.2023.11.262.
[15] H. Li, W. Wei, T. Zhang, F. Liu, X. Xu, Z. Li, Z. Liu, Degradation mechanisms and mitigation strategies of direct methane solid oxide fuel cells, Appl. Energy 359 (2024) 122609, https://doi.org/10.1016/j.apenergy.2023.122609.
[16] J. Zheng, S. Impeng, J. Liu, J. Deng, D. Zhang, Mo promoting Ni-based catalysts confined by halloysite nanotubes for dry reforming of methane: Insight of coking and H2S poisoning resistance, Appl Catal B 342 (2024) 123369, https://doi.org/10.1016/j.apcatb.2023.123369.
[17] H.H. Faheem, B. Britt, M. Rocha, S.-H. Zhou, C.E. Li, W. Cai, L. Fan, Sensitivity analysis and process optimization for biomass processing in an integrated gasifier-solid oxide fuel cell system, Fuel 356 (2024) 129529, https://doi.org/10.1016/j.fuel.2023.129529.
[18] P. Yang, Y. Zhang, C. Yang, J. Chen, Z. Liu, C. Deng, S. Yang, Thermodynamic performance comparison of a SOFC system integrated with steam reforming and dry reforming by utilizing different fuels, Energ. Conver. Manage. 300 (2024) 117981, https://doi.org/10.1016/j.enconman.2023.117981.
[19] S.F. Cannone, M. Ishaq, A. Lanzini, M. Santarelli, Thermodynamic analysis of a synergistic integration of solid oxide fuel cell and solar-based chemical looping methane reforming unit for solar energy storage, power production, and carbon capture, Energ. Conver. Manage. 302 (2024) 118080, https://doi.org/10.1016/j.enconman.2024.118080.
[20] G. Tamburrano, D. Pumiglia, A. Monforti Ferrario, F. Santoni, D. Borello, Analysis of the performances of a solid oxide fuel cell fed by biogas in different plant configurations: An integrated experimental and simulative approach, Int. J. Hydrogen Energy 52 (2024) 745–760, https://doi.org/10.1016/j.ijhydene.2023.07.324.
[21] T. Ouyang, M. Zhang, P. Qin, W. Liu, X. Shi, Converting waste into electric energy and carbon fixation through biosyngas-fueled SOFC hybrid system: A simulation study, Renew. Energy 193 (2022) 725–743, https://doi.org/10.1016/j.renene.2022.05.039.
[22] M. Choolaei, Q. Cai, B. Amini Horri, Green synthesis and characterisation of nanocrystalline NiO-GDC powders with low activation energy for solid oxide fuel cells, Ceram. Int. 47 (23) (2021) 32804–32816, https://doi.org/10.1016/j.ceramint.2021.08.177.
[23] P. Qiu, S. Sun, X. Yang, F. Chen, C. Xiong, L. Jia, J. Li, A review on anode on-cell catalyst reforming layer for direct methane solid oxide fuel cells, Int. J. Hydrogen Energy 46 (49) (2021) 25208–25224, https://doi.org/10.1016/j.ijhydene.2021.05.040.
[24] Z. Lyu, H. Li, M. Han, Electrochemical properties and thermal neutral state of solid oxide fuel cells with direct internal reforming of methane, Int. J. Hydrogen Energy 44 (23) (2019) 12151–12162, https://doi.org/10.1016/j.ijhydene.2019.03.048.
[25] M.A. Abdelkareem, W.H. Tanveer, E.T. Sayed, M.E.H. Assad, A. Allagui, S.W. Cha, On the technical challenges affecting the performance of direct internal reforming biogas solid oxide fuel cells, Renew. Sustain. Energy Rev. 101 (2019) 361–375, https://doi.org/10.1016/j.rser.2018.10.025.
[26] A. Thallam Thattai, L. van Biert, P.V. Aravind, On direct internal methane steam reforming kinetics in operating solid oxide fuel cells with nickel-ceria anodes, J. Power Sources 370 (2017) 71–86, https://doi.org/10.1016/j.jpowsour.2017.09.082.
[27] L. Fan, A. Mokhov, S.A. Saadabadi, N. Brandon, P.V. Aravind, Methane steam reforming reaction in solid oxide fuel cells: Influence of electrochemical reaction and anode thickness, J. Power Sources 507 (2021) 230276, https://doi.org/10.1016/j.jpowsour.2021.230276.
[28] S.-H. Zhou, E. Omanga, A.N. Tabish, W. Cai, L. Fan, Effect of electrochemical reaction on steam adsorption during methane reforming on a Ni-GDC anode, Fuel 332 (2023) 125973, https://doi.org/10.1016/j.fuel.2022.125973.
[29] M. Wójcik, Ł. Szabłowski, O. Dybiński, Comparison of mathematical models of steam methane reforming process for the needs of fuel cells, Int. J. Hydrogen Energy 52 (2024) 965–982, https://doi.org/10.1016/j.ijhydene.2023.08.293.
[30] M.A. Vannice Kinetic Data Analysis and Evaluation of Model Parameters for Uniform (Ideal) Surfaces M.A. Vannice Kinetics of Catalytic Reactions 2005 Springer, US, Boston, MA 106 140 10.1007/978-0-387-25972-7_6.
[31] T.R. Ribeiro, J.B. Ferreira Neto, C. Takano, J.G.R. Poço, L. Kolbeinsen, E. Ringdalen, C-O–H2 ternary diagram for evaluation of carbon activity in CH4-containing gas mixtures, J. Mater. Res. Technol. 13 (2021) 1576–1585, https://doi.org/10.1016/j.jmrt.2021.05.033.
[32] K. Ahmed, K. Föger, Analysis of equilibrium and kinetic models of internal reforming on solid oxide fuel cell anodes: Effect on voltage, current and temperature distribution, J. Power Sources 343 (2017) 83–93, https://doi.org/10.1016/j.jpowsour.2017.01.039.
[33] A. Sciazko, Y. Komatsu, G. Brus, S. Kimijima, J.S. Szmyd, A novel approach to the experimental study on methane/steam reforming kinetics using the Orthogonal Least Squares method, J. Power Sources 262 (2014) 245–254, https://doi.org/10.1016/j.jpowsour.2014.03.097.
[34] L. van Biert, K. Visser, P.V. Aravind, Intrinsic methane steam reforming kinetics on nickel-ceria solid oxide fuel cell anodes, J. Power Sources 443 (2019) 227261, https://doi.org/10.1016/j.jpowsour.2019.227261.
[35] D.J. Moon, J.W. Ryu, Electrocatalytic reforming of carbon dioxide by methane in SOFC system, Catal. Today 87 (1) (2003) 255–264, https://doi.org/10.1016/j.cattod.2003.10.017.
[36] E.O. Voit, H.A. Martens, S.W. Omholt, 150 Years of the Mass Action Law: e1004012, PLoS Comput. Biol. 11 (1) (2015), https://doi.org/10.1371/journal.pcbi.1004012.
[37] Y. Xie, H. Ding, X. Xue, Direct methane fueled solid oxide fuel cell model with detailed reforming reactions, Chemical engineering journal (Lausanne, Switzerland 228 (2013) (1996) 917–924, https://doi.org/10.1016/j.cej.2013.05.084.
[38] M.A. Alsaffar, B.V. Ayodele, J.M. Ali, M.A. Abdel Ghany, S.I. Mustapa, C.K. Cheng, Kinetic modeling and reaction pathways for thermo-catalytic conversion of carbon dioxide and methane to hydrogen-rich syngas over alpha-alumina supported cobalt catalyst, International Journal of Hydrogen Energy 46(60) (2021) 30871-30881. https://doi.org/https://doi.org/10.1016/j.ijhydene.2021.04.158.
[39] Ş. Özkara-Aydınoğlu, A. Erhan Aksoylu, A comparative study on the kinetics of carbon dioxide reforming of methane over Pt–Ni/Al2O3 catalyst: Effect of Pt/Ni Ratio, Chemical Engineering Journal 215–216 (2013) 542–549, https://doi.org/10.1016/j.cej.2012.11.034.
[40] K. Yamamoto, K. Sakaguchi, Hydrogen reactivity factor and effects of oxygen on methane conversion rate by chemical equilibrium calculation, International Journal of Thermofluids 15 (2022) 100186, https://doi.org/10.1016/j.ijft.2022.100186.
[41] R.Y. Chein, W.H. Hsu, C.T. Yu, Parametric study of catalytic dry reforming of methane for syngas production at elevated pressures, Int. J. Hydrogen Energy 42 (21) (2017) 14485–14500, https://doi.org/10.1016/j.ijhydene.2017.04.110.
[42] L. Barelli, G. Bidini, G. Cinti, Steam vs. Dry Reformer: Experimental Study on a Solid Oxide Fuel Cell Short Stack, Catalysts 8 (12) (2018) 599.
[43] H.H. Faheem, S.Z. Abbas, A.N. Tabish, L. Fan, F. Maqbool, A review on mathematical modelling of Direct Internal Reforming- Solid Oxide Fuel Cells, J. Power Sources 520 (2022) 230857, https://doi.org/10.1016/j.jpowsour.2021.230857.
[44] S.A. Saadabadi, B. Illathukandy, P.V. Aravind, Direct internal methane reforming in biogas fuelled solid oxide fuel cell; the influence of operating parameters, Energy Sci. Eng. 9 (8) (2021) 1232–1248, https://doi.org/10.1002/ese3.887.
[45] T. Zhu, Z. Yang, M. Han, Performance evaluation of solid oxide fuel cell with in-situ methane reforming, Fuel 161 (2015) 168–173, https://doi.org/10.1016/j.fuel.2015.08.050.
[46] N. Gokon, Y. Osawa, D. Nakazawa, T. Kodama, Kinetics of CO2 reforming of methane by catalytically activated metallic foam absorber for solar receiver-reactors, Int. J. Hydrogen Energy 34 (4) (2009) 1787–1800, https://doi.org/10.1016/j.ijhydene.2008.12.018.
[47] S.A. Saadabadi, A. Thallam Thattai, L. Fan, R.E.F. Lindeboom, H. Spanjers, P. V. Aravind, Solid oxide fuel cells fuelled with biogas: potential and constraints, Renewable energy 134 (2019) 194–214.
[48] L. Fan, E. Dimitriou, M.J.B.M. Pourquie, M. Liu, A.H.M. Verkooijen, P.V. Aravind, Prediction of the performance of a solid oxide fuel cell fuelled with biosyngas: influence of different steam-reforming reaction kinetic parameters, Int. J.

Hydrogen Energy 38 (1) (2013) 510–524, https://doi.org/10.1016/j.ijhydene.2012.09.061.
[49] X. Wang, Y. Ling, F. Zhou, P. Feng, S. Wang, Efficient conversion of low-concentration coal mine methane by solid oxide fuel cell with in-situ formed nanocomposite catalyst, J. Power Sources 537 (2022) 231521, https://doi.org/10.1016/j.jpowsour.2022.231521.
[50] L.P. Teh, H.D. Setiabudi, S.N. Timmiati, M.A.A. Aziz, N.H.R. Annuar, N.N. Ruslan, Recent progress in ceria-based catalysts for the dry reforming of methane: A review, Chem. Eng. Sci. 242 (2021) 116606, https://doi.org/10.1016/j.ces.2021.116606.
[51] L. Maier, B. Schädel, K. Herrera Delgado, S. Tischer, O. Deutschmann, Steam reforming of methane over nickel: development of a multi-step surface reaction mechanism, Top. Catal. 54 (13) (2011) 845, https://doi.org/10.1007/s11244-011-9702-1.
[52] B. Abdullah, N.A. Abd Ghani, D.-V.-N. Vo, Recent advances in dry reforming of methane over Ni-based catalysts, Journal of Cleaner Production 162 (2017) 170–185, https://doi.org/10.1016/j.jclepro.2017.05.176.
[53] L. Fan, L. van Biert, A. Thallam Thattai, A.H.M. Verkooijen, P.V. Aravind, Study of Methane Steam Reforming kinetics in operating Solid Oxide Fuel Cells: Influence of current density, International Journal of Hydrogen Energy 40(15) (2015) 5150-5159. https://doi.org/https://doi.org/10.1016/j.ijhydene.2015.02.096.
[54] F. Minette, M. Lugo-Pimentel, D. Modroukas, A.W. Davis, R. Gill, M.J. Castaldi, J. De Wilde, Intrinsic kinetics of steam methane reforming on a thin, nanostructured and adherent Ni coating, Appl Catal B 238 (2018) 184–197, https://doi.org/10.1016/j.apcatb.2018.07.015.
[55] B. ℗Łosiewicz, Electrocatalysts for hydrogen energy, Trans Tech Publications 2015 Plaffikon, Switzerland.
[56] M. Wójcik, Ł. Szabłowski, O. Dybiński, Comparison of mathematical models of steam methane reforming process for the needs of fuel cells, Int. J. Hydrogen Energy (2023), https://doi.org/10.1016/j.ijhydene.2023.08.293.
[57] M. Yusuf, M. Beg, M. Ubaidullah, S.F. Shaikh, L.K. Keong, K. Hellgardt, B. Abdullah, Kinetic studies for DRM over high-performance Ni–W/Al2O3–MgO catalyst, Int. J. Hydrogen Energy 47 (100) (2022) 42150–42159, https://doi.org/10.1016/j.ijhydene.2021.08.021.
[58] D. Zambrano, J. Soler, J. Herguido, M. Menéndez, Kinetic study of dry reforming of methane Over Ni–Ce/Al2O3 catalyst with deactivation, Top. Catal. 62 (5) (2019) 456–466, https://doi.org/10.1007/s11244-019-01157-2.